Letter

Anomalous Shiba states in topological iron-based superconductors

Areg Ghazaryan,[1] Ammar Kirmani,[2] Rafael M. Fernandes,[3] and Pouyan Ghaemi[2,4]
[1]*Institute of Science and Technology Austria, Am Campus 1, 3400 Klosterneuberg, Austria*
[2]*Physics Department, City College of the City University of New York, New York, New York 10031, USA*
[3]*School of Physics and Astronomy, University of Minnesota, Minneapolis, Minnesota 55455, USA*
[4]*Physics Program, Graduate Center of City University of New York, New York, New York 10031, USA*

(Received 8 August 2022; accepted 9 November 2022; published 16 November 2022)

We demonstrate the formation of robust zero-energy modes close to magnetic impurities in the iron-based superconductor $FeSe_{1-x}Te_x$. We find that the Zeeman field generated by the impurity favors a spin-triplet interorbital pairing as opposed to the spin-singlet intraorbital pairing prevalent in the bulk. The preferred spin-triplet pairing preserves time-reversal symmetry and is topological, as robust, topologically protected zero modes emerge at the boundary between regions with different pairing states. Moreover, the zero modes form Kramers doublets that are insensitive to the direction of the spin polarization or to the separation between impurities. We argue that our theoretical results are consistent with recent experimental measurements on $FeSe_{1-x}Te_x$.

DOI: 10.1103/PhysRevB.106.L201107

Introduction. Topological superconductivity (TSC) is a quantum state that has been extensively explored [1–3], particularly due to its application for realizing Majorana zero modes (MZMs) [4,5]. In recent years, the iron-based superconductor $FeSe_{1-x}Te_x$ (FST) emerged as a promising candidate for TSC [6]. It was theoretically predicted that the band inversion in the electronic structure of FST can lead to localized MZMs at the end of vortex lines in the superconducting phase [7]. One of the appeals of superconducting FST is the comparable energy scales between the superconducting gap and the Fermi energy, which leads to a wide spectral resolution of the vortex zero mode [8]. The experimental observation of such vortex zero modes has led to extensive studies of FST as a bulk TSC [9–13]. The interplay between topology, superconductivity, and magnetism has also been investigated in relation to surface states and generating new superconducting order [14–19]. On the other hand, several of the properties of FST, such as the existence of vortices with and without zero modes in the same sample, have been puzzling [12,20–23].

Another type of in-gap states in superconductors are the Shiba states, which form near magnetic impurities [24–26]. In certain regimes in-gap states can also be formed for nonmagnetic impurity [27] even when the system respects time-reversal symmetry [28,29]. In FST, in-gap states have been observed near interstitial Fe atoms [30], which behave as magnetic impurities [31]. Interestingly, several of the properties of these in-gap states are different from those of conventional Shiba states. First, Shiba states generally have a finite energy unless the microscopic properties of the superconductor and the coupling strength of the magnetic impurity with the itinerant electrons are fine tuned [32]. Yet in FST the in-gap states at many of the magnetic impurities are observed at zero energy [30,33]. The other surprising property is the absence of a hybridization gap in the Shiba-state energies of two nearby magnetic impurities [30], which contrasts with the standard behavior seen in conventional systems [34]. Scanning tunneling microscopy (STM) measurements have further shown that, while the energy of the in-gap state is zero when the impurity is at the center of the unit cell, it becomes finite when the impurity is pushed toward the edge of the unit cell [33]. Proposals such as anomalous quantum vortices forming at magnetic impurities [35] or effective π-phase shifts at the impurity sites [36,37] have been put forward, but a comprehensive description of the properties of these states is still lacking.

In this Letter we present an alternative mechanism for the formation of zero-energy states close to magnetic impurities in FST. The key property of FST leading to the type of in-gap states discussed in this Letter is the possible existence of multiple superconducting pairing instabilities energetically close to each other. Near an impurity, the Zeeman field generated by it strongly impacts this balance between different types of pairing. In particular, by solving the linearized gap equations, we find that the pairing state favored by the Zeeman field in this region is topologically distinct from the pairing state in regions farther than a multiple lattice spacing from the magnetic impurity. As a result, a pair of zero-energy states form in the boundary region between the two types of pairing. The resulting zero-energy states form bubbles surrounding the magnetic impurity, with a radius of the order of multiple lattice spacing. Since these states arise from the topological character of the superconducting state, their energy is generally pinned at zero.

When two impurities approach each other, the regions around them where the topological superconductivity is dominant merge. As a result, the zero modes surround a larger area and do not become gapped. Furthermore, the type of pairing that is preferred close to the impurity is determined by the symmetries of the system. Therefore, the position of the impurity in the unit cell can affect the type of pairing

selected and, consequently, the development of zero modes. Interestingly, the triplet superconducting pairing that forms close to the magnetic impurity is time-reversal symmetric, and the boundary states are Kramers pairs that are insensitive to the direction of the spin polarization of the magnetic impurity. The latter property is consistent with results from spin-polarized STM measurements [38]. Recently, it has been also shown that the magnetic impurities with strong enough coupling can lead to a π phase shift in the regions close to the impurity on the surface of the material. Such a phase shift will then lead to the formation of a Kramers pair of zero-energy states [36]. In contrast, the mechanism presented in this Letter leads to the change of form of the pairing rather than just the phase of the order parameter. Another feature of the magnetic-impurity-induced in-gap state in FST is that it becomes gapped once the magnetic impurity approaches a magnetic vortex [33]. This is because the two zero modes enclosing the magnetic impurity hybridize in the presence of a Zeeman field. Therefore, due to the vortex hosting a sizable magnetic field, it gaps out the zero modes.

Model Hamiltonian. FST is a member of the family of iron-based superconductors [39] with nonsymmorphic $P4/nmm$ space group symmetry due to the buckling of the chalcogen atoms inside the 2-Fe unit cell [40–42]. At the Γ point, the $P4/nmm$ space group is isomorphic to the D_{4h} point group. The generators of the D_{4h} group can be taken to be π_x, π_z, and π_X reflection planes. Here, x and y connect nearest-neighbor Fe atoms, whereas X and Y, rotated by 45° with respect to x and y, connect next-nearest-neighbor Fe atoms. The FeSe layers are stacked along z. The band structure close to the Γ point mainly contains p_z, d_{xz}, and d_{yz} orbitals and the most general effective Hamiltonian including spin-orbit coupling (SOC) can be constructed using the method of invariants [43,44]. The inversion-odd p_z orbital is essential for realizing band inversion along the Γ-Z direction and thus the nontrivial topology of the band structure [7,42]. In the basis $\psi_{\mathbf{k}} = (|d_+\uparrow\rangle, |d_-\uparrow\rangle, |p_z\uparrow\rangle, |d_+\downarrow\rangle, |d_-\downarrow\rangle, |p_z\downarrow\rangle)$, where $d_\pm = (d_{yz} \pm id_{xz})^T$, the Hamiltonian is given by [42]

$$H(\mathbf{k}) = \sigma_0 \otimes H_0(\mathbf{k}) + H_{\mathrm{SOC}}(\mathbf{k}), \tag{1}$$

where for small in-plane momentum

$$H_0(\mathbf{k}) = \begin{pmatrix} M_1(\mathbf{k}) & \beta k_+^2 & \delta k_- \\ \beta k_-^2 & M_1(\mathbf{k}) & -\delta k_+ \\ \delta k_+ & -\delta k_- & M_2(\mathbf{k}) \end{pmatrix}, \tag{2}$$

with $k_\pm = k_x \pm ik_y$ and $M_n(\mathbf{k}) = E_n + (k_x^2 + k_y^2)/2m_{nx} + t_{nz}[1 - \cos(k_z)]$.

The nonzero elements of the SOC Hamiltonian $H_{\mathrm{SOC}}(\mathbf{k})$ are $H^{22}_{\mathrm{SOC}}(\mathbf{k}) = H^{44}_{\mathrm{SOC}}(\mathbf{k}) = -H^{11}_{\mathrm{SOC}}(\mathbf{k}) = -H^{55}_{\mathrm{SOC}}(\mathbf{k}) = \lambda_1$, and $H^{16}_{\mathrm{SOC}}(\mathbf{k}) = H^{35}_{\mathrm{SOC}}(\mathbf{k}) = \sqrt{2}\lambda_3 \sin(k_z)$, as well as the matrix elements related by Hermiticity. The parameters β, δ, E_1, E_2, m_1, m_2, t_1, t_2, λ_1, and λ_3 were previously determined using density functional theory [7].

Symmetries and pairing states. The types of pairing states in FST can be classified according to irreducible representations of the D_{4h} symmetry group of the underlying lattice [45]. D_{4h} has five odd-parity and five even-parity irreducible representations. We only consider pairing with zero center-of-mass momentum. In the even sector, the standard pairing is intraorbital spin singlet that transforms as the A_{1g} representation and has the form $\Delta_1 : \sigma_0 \otimes \mathbf{1}_3$. We use the standard Bogoliubov–de Gennes (BdG) basis where the wave function has the form $\Psi_{\mathbf{k}} = (\psi_{\mathbf{k}}, i\sigma_y K\psi_{\mathbf{k}})^T$. Due to the presence of SOC, there is a spin-triplet interorbital pairing involving the d_{xz} and d_{yz} orbitals that also transforms as A_{1g}, of the form $\sigma_z d_{xz} d_{yz}$. This pairing state, favored by the Hund's coupling [46], does not pair the p_z orbitals. Therefore, when the chemical potential is close to the p-d band inversion point, the $\sigma_z d_{xz} d_{yz}$ pairing state is not energetically favorable.

On the other hand, there are four types of odd-parity pairing states that are interorbital triplet and involve the p_z orbital. They are $\Delta_{2\pm} : \sigma_x p_z d_{xz} \pm \sigma_y p_z d_{yz}$, which transforms as the A_{1u} (+) or B_{1u} (−) irreducible representation, and $\Delta_{3\pm} : \sigma_y p_z d_{xz} \mp \sigma_x p_z d_{yz}$, which transforms as A_{2u} (+) or B_{3u} (−). In the $d_\pm$ basis, these gap functions generate the Bogoliubov–de Gennes mean-field pairing terms,

$$H_{\Delta_{\{2,3\},+}} = \Delta_{\{2,3\},+} i^{\{0,1\}} \tau_x \begin{pmatrix} 0 & 0 & 0 & 0 & 0 & 1 \\ 0 & 0 & 0 & 0 & 0 & 0 \\ 0 & 0 & 0 & 0 & -1 & 0 \\ 0 & 0 & 0 & 0 & 0 & 0 \\ 0 & 0 & \mp 1 & 0 & 0 & 0 \\ \pm 1 & 0 & 0 & 0 & 0 & 0 \end{pmatrix}, \tag{3}$$

$$H_{\Delta_{\{2,3\},-}} = \Delta_{\{2,3\},-} i^{\{0,1\}} \tau_x \begin{pmatrix} 0 & 0 & 0 & 0 & 0 & 0 \\ 0 & 0 & 0 & 0 & 0 & 1 \\ 0 & 0 & 0 & -1 & 0 & 0 \\ 0 & 0 & \mp 1 & 0 & 0 & 0 \\ 0 & 0 & 0 & 0 & 0 & 0 \\ 0 & \pm 1 & 0 & 0 & 0 & 0 \end{pmatrix}, \tag{4}$$

where the upper (lower) signs refer to Δ_2 (Δ_3) and the Pauli matrix τ_j acts in Nambu particle-hole space. The overall phase was chosen such that both $\Delta_{2,\pm}$ and $\Delta_{3,\pm}$ respect time-reversal symmetry.

From a numerical analysis, we identify that all these pairing states, except Δ_{2+}, are nodal. The structure of the pairing gaps has important implications for the topological character of the superconducting state. Indeed, a time-reversal and odd-parity pairing is topological if it is gapped and encloses an odd number of time-reversal invariant momenta [47]. The space group $P4/nmm$ has nonsymmorphic symmetry operation inversion followed by half translation, which at the Γ point corresponds to the inversion symmetry operation of D_{4h} [41]. As a result, the triplet pairings of FST identified above, $\Delta_{2\pm}$ and $\Delta_{3\pm}$, have odd parity. Since only Δ_{2+} has a full gap, it is the only one among those four that can be in a topological superconducting state, as long as it encloses an odd number of time-reversal invariant momenta.

Effect of the Zeeman field. To determine the dominant pairing instability as a function of the Zeeman field we utilize the linearized gap equation [48]. We start by defining the finite temperature superconducting susceptibilities,

$$\chi_{lm} = -\frac{T}{N} \sum_{\omega_n \mathbf{p}} \mathrm{Tr}\left[\frac{H^\dagger_{\Delta_l}}{\Delta_l} G_0(i\omega_n, \mathbf{p}, \Delta_Z) \times \frac{H_{\Delta_m}}{\Delta_m} G_0(-i\omega_n, \mathbf{p}, -\Delta_Z) \right], \tag{5}$$

where H_{Δ_l} is the pairing Hamiltonian, N is the number of momentum points, and $G_0(i\omega_n, \mathbf{p}, \Delta_z) = \sum_j \mathcal{P}_{j\mathbf{p}\Delta_Z}/(i\omega_n - \epsilon_{j\mathbf{p}\Delta_z})$ is the normal state Green's function. j runs through the bands, ω_n is the Matsubara frequencies, and $\mathcal{P}_{j,\mathbf{p}\Delta_Z}$ is the projection operator onto band j at momentum $\mathbf{p}$. The Zeeman-field energy splitting is Δ_Z. Finally, the subscripts l and m label the five pairing states discussed above: the singlet Δ_1 and the triplets $\Delta_{2\pm}$, $\Delta_{3\pm}$. The linearized gap equations, which determine the critical temperature T_c for each pairing instability, take the form

$$-\frac{1}{g_s} - \chi_{11} = 0, \tag{6}$$

$$-\frac{2}{3g_t} - \chi_{tt} = 0, \tag{7}$$

where g_l are the superconducting coupling constants arising from the microscopic interactions, with $s = 1$ and $t = \pm 2, \pm 3$. In deriving these expressions, we ignored mixing between different pairing channels, e.g., Δ_{2+} and Δ_{2-}, that is allowed by the Zeeman field. We will justify this later.

To proceed, we need to discuss the coupling constants g_l. We assume, without specifying a mechanism, that there is an attractive interaction in the singlet channel, since this is the state realized in the bulk. As for the triplet states, according to what we discussed above, only Δ_{2+} can correspond to a topological pairing state, which can display zero-energy modes. It is therefore crucial to identify the microscopic interactions that favor $g_{2\pm}$ over $g_{3\pm}$. We start from a generalized Hubbard-Kanamori interacting Hamiltonian [49–51] for the p_z, d_{xz}, and d_{yz} orbitals, which includes anisotropic Hund's terms J_1, J_2, and J_3. We find a simple condition under which there is an effective attractive interaction only for the $\Delta_{2\pm}$ states (see Supplemental Material [52]): $J_1 > J_2$ and $J_3 + J_1 - J_2 < V < J_3 + J_2 - J_1$, where V is the interorbital Hubbard repulsion. We assume this condition is satisfied, set $g_{2\pm} = g_t$, and focus hereafter on the $\Delta_{2\pm}$ and Δ_1 states only.

Figure 1(a) shows the phase boundaries for the different pairing states in the parameter space of Zeeman splitting and the coupling constant ratio g_t/g_s. The Zeeman field is taken in the $\hat{\mathbf{z}}$ or $\hat{\mathbf{x}}$ (in-plane) direction. The phase boundaries between Δ_{2+} and Δ_{2-} are quite separated, such that Δ_{2+} dominates for small values of the coupling constant ratio, regardless of the field direction. This not only shows that Δ_{2+} is the favored pairing state for larger Zeeman coupling, but also that the Zeeman-induced mixing with Δ_{2-} should be small, which justifies dropping this term in the gap equations. Figure 1(a) shows that the phase boundary is almost insensitive to the direction of the Zeeman field.

To show that Δ_{2+} pairing is robust with respect to changes in the chemical potential, Figs. 1(b) and 1(c) show the small changes experienced by the Δ_{2+}-Δ_1 phase boundary for four different values of μ. Therefore, upon increasing the Zeeman coupling, the pairing state will transition from intraorbital singlet Δ_1 to interorbital triplet Δ_{2+}.

While the preferred pairing is robust with respect to the chemical potential modification, its topological nature depends on the chemical potential. The relevant time-reversal invariant momenta are at the Γ and Z points. For $\mu > -0.577$ eV, the Fermi surface at the Z point is filled, whereas

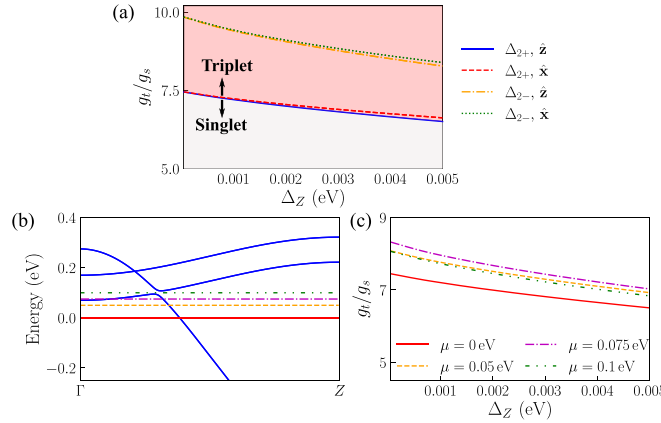

FIG. 1. (a) Phase boundary between different interorbital triplet ($\Delta_{2\pm}$) and intraorbital spin-singlet (Δ_1) pairing states for $\mu = 0$ eV when the Zeeman field is along the $\hat{\mathbf{z}}$ or $\hat{\mathbf{x}}$ direction. Singlet (triplet) pairing emerges in the light gray (light red) region, following the phase boundary for the Zeeman field along the $\hat{\mathbf{z}}$ direction. (b) Band structure in the Γ-Z direction. The selected chemical potentials are those for which the phase boundaries between Δ_{2+} and Δ_1 are shown in (c). The Zeeman field is in the $\hat{\mathbf{z}}$ direction for (c).

for $\mu < 0.07$ eV, all three bands at Γ are empty. Therefore, in this range of μ, the Δ_{2+} pairing state is topological. Consequently, in Figs. 1(c) and 1(d), only two chemical potential values $\mu = 0$ eV and $\mu = 0.05$ eV correspond to a topological superconductor. The cases $\mu = 0.075$ eV and $\mu = 0.1$ eV are generally nontopological. For $\mu = 0.075$ eV, the lowest band at the Γ point is quite close to the Fermi energy. As a result, a topological phase transition can be induced by increasing the pairing amplitude or further tuning the chemical potential. Since this requires considerable tuning, difficult to achieve experimentally, we focus on values of the chemical potential where Δ_{2+} is strictly topological.

When the chemical potential is in the band-inversion gap, the normal state itself is topological [7] [see Fig. 1(c)]. This is manifested by Majorana bound states at the end of the vortex cores where they cross the sample boundary [10,53]. In this case, the bulk pairing state is intraorbital spin-singlet Δ_1 which is not topological in the bulk, but it also induces topological superconductivity on the surface [53]. Since our interest is in the vicinity of bulk impurities, we will not discuss surface effects.

Majorana modes. Having identified the dominant pairing state in the presence of Zeeman coupling, we now examine the possible boundary mode localized between regions with Δ_{2+} and spin-singlet Δ_1 pairings. Since for a considerable range of chemical potential values the Δ_{2+} pairing is topological, the presence of zero-energy edge modes is expected. The Δ_{2+} pairing respects time-reversal symmetry, therefore the zero modes are Kramers pairs with opposite spin.

Figures 2 and 3 depict the structure of zero modes for single and double magnetic impurities. Figures 2(a) and 2(b) show the case of a single Fe impurity. The effective magnetic field generated by the magnetic impurity modifies the superconducting order parameter in its surroundings, such that Δ_{2+} pairing is realized. The boundary with the bulk singlet pairing features zero-energy modes. Therefore, scanning tunneling

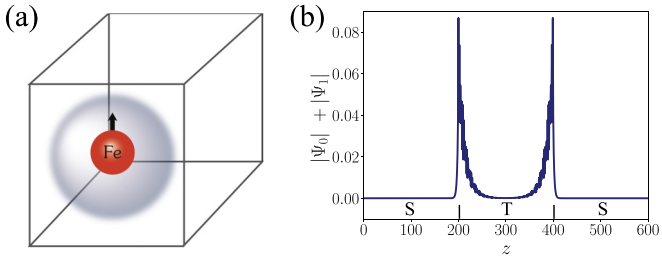

FIG. 2. (a) Schematic representation of the interstitial Fe atom and its surrounding triplet pairing state, separated from the spin-singlet pairing realized away from the atom. (b) Corresponding total probability distribution, along the $\hat{\mathbf{z}}$ direction, for the zero-energy mode Kramers pair. The system size is 600 lattice sites, divided into three regions of singlet/triplet (topological)/singlet pairings with 200 sites each. The chemical potential is $\mu = 0$ meV, and $k_x = k_y = 0$.

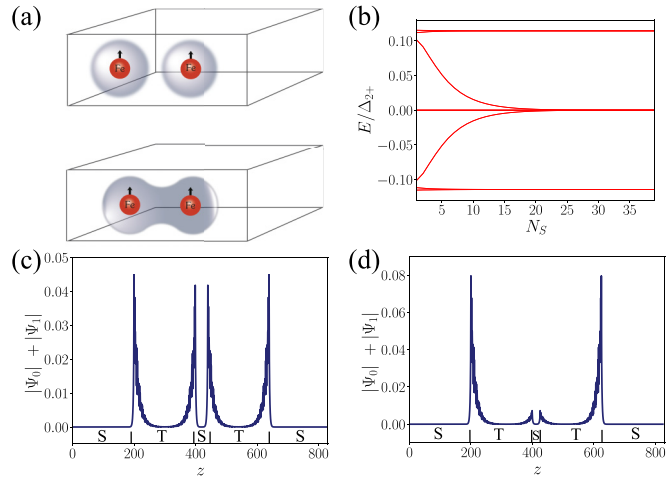

FIG. 3. (a) Schematic representation of bringing two interstitial Fe atoms closer. (b) Dependence of the in-gap energy states on the effective two-impurity separation in the $\hat{\mathbf{z}}$ direction. The two-impurity state is simulated by a five-region sandwich with superconducting pairings singlet/triplet/singlet/triplet/singlet; the distance between the boundaries of the two triplet regions is N_S sites. (c), (d) Corresponding total probability when two Fe atoms are farther apart and closer to each other, respectively. For (c) and (d) the system is the same as in (b) with $N_S = 25$ for (c) and $N_S = 40$ for (d). The chemical potential is $\mu = 0$ meV and $k_x = k_y = 0$.

spectroscopy close to the interstitial iron atom should detect a robust zero-bias peak [30,33,38]. The observed zero mode is different from usual Shiba state observed next to a magnetic impurity [32], whose energy depends on the amplitude of the exchange interaction and requires special tuning to be fixed at zero energy. In contrast, in our case, as long as the magnetic field is sufficiently large to favor topological Δ_{2+} pairing, the zero-energy mode is robust.

Figure 3 shows the evolution of the zero modes when the two impurities are brought close to each other. As shown in Fig. 3(b), while two of the zero modes are gapped out, the ones located on the outer edge of the two-impurity region remain robust. This is consistent with the experimental observation in Ref. [30] and is different from the expected hybridization between Shiba states when the two impurities are brought close to each other. This shows that the corresponding zero modes form bubbles around the magnetic impurities, which combine into a single bubble enclosing both atoms when the impurities are close to each other.

Finally, we comment on the size of the bubble formed around the interstitial magnetic impurity. Analyzing the Friedel oscillations from neutron scattering data, Ref. [31] used a five-orbital Hubbard model to estimate that the nearest-neighbor spin exchange between the interstitial and the surrounding Fe atoms is about 70 meV. This is an order of magnitude larger than the Zeeman field required to observe the triplet pairing state and the topological superconducting region around the magnetic impurity (see Fig. 1). Therefore, despite the exchange interaction being short ranged, we expect the radius of the bubble to be in the range of a multiple lattice spacing, consistent with experimental observations [30].

Conclusions. We have shown that the peculiar features of the zero-bias peak experimentally observed at interstitial iron atoms in FST can be reconciled if we consider the modification of the superconducting order parameter close to the impurity. We have shown that the Zeeman field prefers interorbital triplet pairing which, for a certain range of chemical potential values, is topological. As a result, zero-energy modes naturally occur at the boundary between interorbital triplet and intraorbital singlet pairings. These modes are robust and do not get modified by changes in the exchange interaction, contrary to the conventional Shiba states. It has been experimentally observed that the zero modes are not spin polarized [38], a feature that is also consistent with our theoretical model. The obtained triplet pairing state near the impurity respects time-reversal symmetry, such that the zero modes are always doubly degenerate and have opposite spin due to the Kramers theorem. This mechanism is also capable of explaining the robustness of the zero modes when two impurities are brought close to each other, since in this case only two out of four modes get hybridized.

We thank A. Rahmani, A. V. Chubukov, J. D. Sau, and R. Zhang for fruitful discussions. A.K. and P.G. are supported by NSF-DMR2037996. P.G. also acknowledges support from NSF-DMR1824265. R.M.F. was supported by the U. S. Department of Energy, Office of Science, Basic Energy Sciences, Materials Sciences and Engineering Division, under Award No. DE-SC0020045. Part of this work was performed at the Aspen Center for Physics, which is supported by National Science Foundation Grant No. PHY-1607611.

[1] M. Z. Hasan and C. L. Kane, Colloquium: Topological insulators, Rev. Mod. Phys. **82**, 3045 (2010).
[2] X.-L. Qi and S.-C. Zhang, Topological insulators and superconductors, Rev. Mod. Phys. **83**, 1057 (2011).
[3] M. Sato and Y. Ando, Topological superconductors: A review, Rep. Prog. Phys. **80**, 076501 (2017).
[4] J. Alicea, New directions in the pursuit of Majorana fermions in solid state systems, Rep. Prog. Phys. **75**, 076501 (2012).

[5] K. Flensberg, F. von Oppen, and A. Stern, Engineered platforms for topological superconductivity and Majorana zero modes, Nat. Rev. Mater. **6**, 944 (2021).

[6] Z. Wang, P. Zhang, G. Xu, L. Zeng, H. Miao, X. Xu, T. Qian, H. Weng, P Richard, A. V. Fedorov, H. Ding, X. Dai, and Z. Fang, Topological nature of the $FeSe_{0.5}Te_{0.5}$ superconductor, Phys. Rev. B **92**, 115119 (2015).

[7] G. Xu, B. Lian, P. Tang, X.-L. Qi, and S.-C. Zhang, Topological Superconductivity on the Surface of Fe-Based Superconductors, Phys. Rev. Lett. **117**, 047001 (2016).

[8] A. Kreisel, P. J. Hirschfeld, and B. M. Andersen, On the remarkable superconductivity of FeSe and its close cousins, Symmetry **12**, 1402 (2020).

[9] P. Zhang, K. Yaji, T. Hashimoto, Y. Ota, T. Kondo, K. Okazaki, Z. Wang, J. Wen, G. Gu, H. Ding, and S. Shin, Observation of topological superconductivity on the surface of an iron-based superconductor, Science **360**, 182 (2018).

[10] D. Wang, L. Kong, P. Fan, H. Chen, S. Zhu, W. Liu, L. Cao, Y. Sun, S. Du, J. Schneeloch, R. Zhong, G. Gu, L. Fu, H. Ding, and H.-J. Gao, Evidence for Majorana bound states in an iron-based superconductor, Science **362**, 333 (2018).

[11] S. Zhu, L. Kong, L. Cao, H. Chen, M. Papaj, S. Du, Y. Xing, W. Liu, D. Wang, C. Shen, F. Yang, J. Schneeloch, R. Zhong, G. Gu, L. Fu, Y.-Y. Zhang, H. Ding, and H.-J. Gao, Nearly quantized conductance plateau of vortex zero mode in an iron-based superconductor, Science **367**, 189 (2020).

[12] T. Machida, Y. Sun, S. Pyon, S. Takeda, Y. Kohsaka, T. Hanaguri, T. Sasagawa, and T. Tamegai, Zero-energy vortex bound state in the superconducting topological surface state of Fe(Se,Te), Nat. Mater. **18**, 811 (2019).

[13] H. Miao, W. H. Brito, Z. P. Yin, R. D. Zhong, G. D. Gu, P. D. Johnson, M. P. M. Dean, S. Choi, G. Kotliar, W. Ku, X. C. Wang, C. Q. Jin, S.-F. Wu, T. Qian, and H. Ding, Universal 2Δ max$/k_BT_c$ scaling decoupled from the electronic coherence in iron-based superconductors, Phys. Rev. B **98**, 020502(R) (2018).

[14] Y. Li, N. Zaki, V. O. Garlea, A. T. Savici, D. Fobes, Z. Xu, F. Camino, C. Petrovic, G. Gu, P. D. Johnson, J. M. Tranquada, and I. A. Zaliznyak, Electronic properties of the bulk and surface states of $Fe_{1+y}Te_{1-x}Se_x$, Nat. Mater. **20**, 1221 (2021).

[15] L.-H. Hu, P. D. Johnson, and C. Wu, Pairing symmetry and topological surface state in iron-chalcogenide superconductors, Phys. Rev. Res. **2**, 022021(R) (2020).

[16] N. Zaki, G. Gu, A. Tsvelik, C. Wu, and P. D Johnson, Time-reversal symmetry breaking in the Fe-chalcogenide superconductors, Proc. Natl. Acad. Sci. USA **118**, e2007241118 (2021).

[17] C. Youmans, A. Ghazaryan, M. Kargarian, and P. Ghaemi, Odd-frequency pairing in the edge states of superconducting pnictides in the coexistence phase with antiferromagnetism, Phys. Rev. B **98**, 144517 (2018).

[18] M. Dzero and A. Levchenko, Impurity bands in magnetic superconductors with spin density wave, Ann. Phys., 168945 (2022).

[19] S. Li, L.-H. Hu, R.-X. Zhang, and S. Okamoto, Topological superconductivity from forward phonon scatterings, arXiv:2207.09443.

[20] Z. Wang, J. O. Rodriguez, L. Jiao, S. Howard, M. Graham, G. D. Gu, T. L. Hughes, D. K. Morr, and V. Madhavan, Evidence for dispersing 1D Majorana channels in an iron-based superconductor, Science **367**, 104 (2020).

[21] C.-K. Chiu, T. Machida, Y. Huang, T Hanaguri, and F.-C. Zhang, Scalable Majorana vortex modes in iron-based superconductors, Sci. Adv. **6**, eaay0443 (2020).

[22] A. Ghazaryan, P. L. S. Lopes, P. Hosur, M. J. Gilbert, and P. Ghaemi, Effect of Zeeman coupling on the Majorana vortex modes in iron-based topological superconductors, Phys. Rev. B **101**, 020504(R) (2020).

[23] L.-H. Hu and R.-X. Zhang, Topological superconducting vortex from trivial electronic bands, arXiv:2204.03175.

[24] L. Yu, Bound state in superconductors with paramagnetic impurities, Acta Phys. Sin. **21**, 75 (1965).

[25] H. Shiba, Classical spins in superconductors, Prog. Theor. Phys. **40**, 435 (1968).

[26] A. I. Rusinov, Superconductivity near paramagnetic impurity, JETP Lett. **9**, 85 (1969).

[27] J. D. Sau and E. Demler, Bound states at impurities as a probe of topological superconductivity in nanowires, Phys. Rev. B **88**, 205402 (2013).

[28] M. Matsumoto, M. Koga, and H. Kusunose, Single impurity effects in multiband superconductors with different sign order parameters, J. Phys. Soc. Jpn. **78**, 084718 (2009).

[29] M. Mashkoori, A. G. Moghaddam, M. H. Hajibabaee, A. M. Black-Schaffer, and F. Parhizgar, Impact of topology on the impurity effects in extended s-wave superconductors with spin-orbit coupling, Phys. Rev. B **99**, 014508 (2019).

[30] J.-X. Yin, Z. Wu, J. H. Wang, Z. Y. Ye, J. Gong, X. Y. Hou, L. Shan, A. Li, X. J. Liang, X. X. Wu, J. Li, C. S. Ting, Z. Q. Wang, J. P. Hu, P. H. Hor, H. Ding, and S. H. Pan, Observation of a robust zero-energy bound state in iron-based superconductor Fe(Te,Se), Nat. Phys. **11**, 543 (2015).

[31] V. Thampy, J. Kang, J. A. Rodriguez-Rivera, W. Bao, A. T. Savici, J. Hu, T. J. Liu, B. Qian, D. Fobes, Z. Q. Mao, C. B. Fu, W. C. Chen, Q. Ye, R. W. Erwin, T. R. Gentile, Z. Tesanovic, and C. Broholm, Friedel-Like Oscillations from Interstitial Iron in Superconducting $Fe_{1+y}Te_{0.62}Se_{0.38}$, Phys. Rev. Lett. **108**, 107002 (2012).

[32] A. V. Balatsky, I. Vekhter, and J.-X. Zhu, Impurity-induced states in conventional and unconventional superconductors, Rev. Mod. Phys. **78**, 373 (2006).

[33] P. Fan, F. Yang, G. Qian, H. Chen, Y.-Y. Zhang, G. Li, Z. Huang, Y. Xing, L. Kong, W. Liu, K. Jiang, C. Shen, S. Du, J. Schneeloch, R. Zhong, G. Gu, Z. Wang, H. Ding, and H.-J. Gao, Observation of magnetic adatom-induced Majorana vortex and its hybridization with field-induced Majorana vortex in an iron-based superconductor, Nat. Commun. **12**, 1348 (2021).

[34] M. Ruby, B. W. Heinrich, Y. Peng, F. von Oppen, and K. J. Franke, Wave-Function Hybridization in Yu-Shiba-Rusinov Dimers, Phys. Rev. Lett. **120**, 156803 (2018).

[35] K. Jiang, X. Dai, and Z. Wang, Quantum Anomalous Vortex and Majorana Zero Mode in Iron-Based Superconductor Fe(Te,Se), Phys. Rev. X **9**, 011033 (2019).

[36] R. Song, P. Zhang, X.-T. He, and N. Hao, Ferromagnetic impurity induced majorana zero mode in iron-based superconductor, arXiv:2203.14017.

[37] K. Björnson, A. V. Balatsky, and A. M. Black-Schaffer, Superconducting order parameter π-phase shift in magnetic impurity wires, Phys. Rev. B **95**, 104521 (2017).

[38] D. Wang, J. Wiebe, R. Zhong, G. Gu, and R. Wiesendanger, Spin-Polarized Yu-Shiba-Rusinov States in an Iron-Based Superconductor, Phys. Rev. Lett. **126**, 076802 (2021).

[39] R. M. Fernandes, A. I. Coldea, H. Ding, I. R. Fisher, P. Hirschfeld, and G. Kotliar, Iron pnictides and chalcogenides: A new paradigm for superconductivity, Nature (London) **601**, 35 (2022).

[40] R. M. Fernandes and A. V. Chubukov, Low-energy microscopic models for iron-based superconductors: A review, Rep. Prog. Phys. **80**, 014503 (2017).

[41] V. Cvetkovic and O. Vafek, Space group symmetry, spin-orbit coupling, and the low-energy effective Hamiltonian for iron-based superconductors, Phys. Rev. B **88**, 134510 (2013).

[42] H. Lohani, T. Hazra, A. Ribak, Y. Nitzav, H. Fu, B. Yan, M. Randeria, and A. Kanigel, Band inversion and topology of the bulk electronic structure in $FeSe_{0.45}Te_{0.55}$, Phys. Rev. B **101**, 245146 (2020).

[43] T. Inui, Y. Tanabe, and Y. Onodera, *Group Theory and its Applications in Physics*, Vol. 78 (Springer, Berlin, 1990).

[44] G. L. Bir and G. E. Pikus, *Symmetry and Strain-Induced Effects in Semiconductors* (Wiley, New York, 1974).

[45] M. Sigrist and K. Ueda, Phenomenological theory of unconventional superconductivity, Rev. Mod. Phys. **63**, 239 (1991).

[46] O. Vafek and A. V. Chubukov, Hund Interaction, Spin-Orbit Coupling, and the Mechanism of Superconductivity in Strongly Hole-Doped Iron Pnictides, Phys. Rev. Lett. **118**, 087003 (2017).

[47] L. Fu and E. Berg, Odd-parity topological superconductors: Theory and application to $Cu_xBi_2Se_3$, Phys. Rev. Lett. **105**, 097001 (2010).

[48] M. H. Fischer, Gap symmetry and stability analysis in the multiorbital Fe-based superconductors, New J. Phys. **15**, 073006 (2013).

[49] J. Kanamori, Electron Correlation and Ferromagnetism of Transition Metals, Prog. Theor. Phys. **30**, 275 (1963).

[50] A. Georges, L. Medici, and J. Mravlje, Strong correlations from Hund's coupling, Annu. Rev. Condens. Matter Phys. **4**, 137 (2013).

[51] S. Graser, T. Maier, P. Hirschfeld, and D. Scalapino, Near-degeneracy of several pairing channels in multiorbital models for the Fe pnictides, New J. Phys. **11**, 025016 (2009).

[52] See Supplemental Material at http://link.aps.org/supplemental/10.1103/PhysRevB.106.L201107 for more details on microscopic interactions.

[53] L. Fu and C. L. Kane, Superconducting Proximity Effect and Majorana Fermions at the Surface of a Topological Insulator, Phys. Rev. Lett. **100**, 096407 (2008).